PCCP

Local Orientation of Chains at Crystal/Amorphous Interfaces Buried in Isotactic Polypropylene Thin Films

Journal:	*Physical Chemistry Chemical Physics*
Manuscript ID	CP-COM-08-2021-003959.R1
Article Type:	Communication
Date Submitted by the Author:	26-Sep-2021
Complete List of Authors:	Kawaguchi, Daisuke; Kyushu University, Applied Chmistry Yamamoto, Kentaro; Kyushu University, Applied Chmistry Abe, Tatsuki; Kyushu University, Applied Chmistry Jiang, Naisheng ; Stony Brook University, Materials Science and Chemical Engineering Koga, Tadanori; Stony Brook University, Chemical and Molecular Engineering Program Yamamoto, Satoru; Kyushu University, Center for Polymer Interface and Molecular Adhesion Science Tanaka, Keiji; Kyushu University, Applied Chemistry

COMMUNICATION

Local Orientation of Chains at Crystal/Amorphous Interfaces Buried in Isotactic Polypropylene Thin Films

Received 00th January 20xx,
Accepted 00th January 20xx

DOI: 10.1039/x0xx00000x

Daisuke Kawaguchi[a,b*], Kentaro Yamamoto[a], Tatsuki Abe[a], Naisheng Jiang[c], Tadanori Koga[c,d], Satoru Yamamoto[b], and Keiji Tanaka[a,b*]

A better understanding of the aggregation states of polymer chains in thin films is of pivotal importance for developing thin film polymer devices in addition to its inherent scientific interest. Here we report the preferential orientation of the crystalline lamellae for *isotactic* polypropylene (*i*PP) in spin-coated films by grazing incidence of wide-angle X-ray diffraction in conjunction with sum frequency generation vibrational spectroscopy, which provides information on the local conformation of chains at crystal/amorphous interfaces buried in a thin film. The crystalline orientation of *i*PP, which formed cross-hatched lamellae induced by lamellar branching, altered from a mixture of edge-on and face-on mother lamellae to preferential face-on mother lamellae with decreasing thickness. The orientation of methyl groups at the crystal/amorphous interfaces in the interior region of the *i*PP films changed, accompanied by a change in the lamellar orientation.

Polymer thin films are used in a wide variety of applications such as microelectronics and biomedical technology.[1] Since polymer chains in a thin film are in a confined state, their aggregation states and thermal molecular motion are different from those in the bulk state.[2-12] This is the case even for semi-crystalline polymers. However, the confinement effect becomes more remarkable than in amorphous ones due to the presence of a hierarchy based on a complicated crystalline structure. A semi-crystalline polymer generally forms three-dimensional spherulites composed of radially directed fibrils, also called lamellar stacks, in the bulk phase. A fibril also consists of crystalline lamellae together with amorphous segments such as chain foldings and tie-molecules. Once the film becomes thinner, the local orientation of even crystalline lamellae may be altered because the crystal growth is also affected by the confinement effect. Thus, to improve the performance of polymer thin film materials and devices, the structure-property relationship of chains in such a confined state must be better understood as a first benchmark.

So far, the orientation of the crystalline lamellae and controlling factors in them have been extensively studied.[13-27] In a thin film of semi-crystalline polymer, the lamellae formed can preferentially orient.[28] The crystalline lamellae, in which the chain axis (*c*-axis) orients along the direction parallel and perpendicular to the substrate surface, are so-called “edge-on” and “face-on” lamellae, respectively. Phenomenologically, the controlling factors in the orientation in the confined state seem to be mainly the interfacial interaction between polymer chains and substrate in addition to the chain diffusion based on the crystallization temperature.[29, 30] The former and latter correspond to the thermodynamic and kinetic factors, respectively. Such information is crucial for an essential understanding of the crystallization behavior of polymers, especially in thin films, and for the design of thin-film devices such as organic field-effect transistors (OFET) and organic solar cells (OSC).[31-41] For example, in the case of poly(3-hexylthiophene) (P3HT), it has been reported that while the edge-on lamellae enhance the carrier mobility along the in-plane direction for OFET,[31, 32, 34] the face-on lamellae perform this function along the out-of-plane direction for OSC.[37, 38]

Meanwhile, structural studies of amorphous chains such as ties, foldings, and tails in semi-crystalline polymer films are limited. Ties are the links between adjacent crystalline lamellae. Foldings, or loops, exit and re-enter the same crystallite. Tails are the end portion of a chain which exit from a crystalline lamella. Among them, ties strongly affect the mechanical properties in semi-crystalline polymers.[42, 43] Taking into account the fact that amorphous chains are chemically connected to the chain in a crystalline phase, it seems reasonable to hypothesize that the chain orientation is dependent on the orientation of the crystalline lamellae.

[a] *Department of Applied Chemistry, Kyushu University, Fukuoka 819-0395, Japan.*
[b] *Center for Polymer Interface and Molecular Adhesion Science, Kyushu University, Fukuoka 819-0395, Japan.*
[c] *Department of Materials Science and Chemical Engineering, Stony Brook University, Stony Brook, New York 11794-2275, United States.*
[d] *Department of Chemistry, Stony Brook University, Stony Brook, New York 11794-3400, United States*

† Footnotes relating to the title and/or authors should appear here.
Electronic Supplementary Information (ESI) available: [details of any supplementary information available should be included here]. See DOI: 10.1039/x0xx00000x

A question to be addressed is how we obtain the depth-dependent information of crystalline lamellae. The crystalline structure in the surface region can be studied by atomic force microscopy (AFM),[44-46] in conjunction with grazing incidence small-angle X-ray scattering (GISAXS) and wide-angle X-ray diffraction (GIWAXD).[47, 48] On the other hand, it is experimentally difficult to gather lamellar information in the interior region. Sum frequency generation (SFG) spectroscopy provides the vibrational information at the location where the centrosymmetry is broken,[49, 50] and has been hitherto applied to various interfaces to delve into the local conformation of chains there.[9, 12, 51-58] If this technique is applicable to a crystal/amorphous interface in the interior region of a semi-crystalline film, the depth-dependent information of crystalline lamellae will be revealed. In this study we examine the orientation of crystalline lamellae of *isotactic* polypropylene (*i*PP), which is one of the representative semi-crystalline polymers, in spin-coated films, using GIWAXD measurements. Then, we apply SFG spectroscopy to discuss the local conformation of *i*PP chains at crystal/amorphous interfaces in the interior region of the films where possible.

As a material, *i*PP kindly supplied by Japan Polychem Corporation was used. The number-average molecular weight (M_n) and polydispersity index (M_w/M_n), where M_w was the weight-average molecular weight, were determined to be 62k and 4.2, respectively, by high-temperature gel permeation chromatography (GPC) with polystyrene (PS) standards and the Q-factor method.[59] The melting temperature (T_m) of *i*PP was 429.7 K (156.6 ℃) by differential scanning calorimetry (DSC, DSC6220, Hitachi High-Tech, Tokyo, Japan) with a heating rate of 10 K•min^{-1}. As a reference, atactic polypropylene (*a*PP) purchased from Sigma Aldrich was also used. M_n and M_w/M_n were 3.4k and 2.7, respectively, by GPC with PS standards. *i*PP was dissolved in *p*-xylene at 411 K (138 ℃). Films of *i*PP were prepared by a spin-coating method from the solution onto quartz prisms (for SFG measurements) and Si wafers (for GIWAXD measurements) kept at 353 K (80 ℃). The *i*PP films were melted at 473 K (200 ℃) and cooled down to room temperature at a cooling rate of approximately 1 K•min^{-1} under vacuum. *a*PP films were prepared by a spin-coating method from a toluene solution kept at 363 K (90 ℃) onto quartz prisms and Si wafers kept at 323 K (50 ℃). To examine the film thickness, all films were partly scratched by a blade so that the substrate was uncovered. The height difference between the scratched- and unscratched-regions obtained by atomic force microscopy was defined as the film thickness. Additional information for the sample preparation and characterization is described in the electronic supplementary information (ESI).

The surface morphology of the *i*PP thin films was observed by AFM (E-sweep; Hitachi High-Tech, Tokyo, Japan). A silicon cantilever (SI-DF20, Hitachi High-Tech, Tokyo, Japan) with a tip radius of 10 nm and a spring constant of 17 N•m^{-1} was used. The crystalline structure of *i*PP thin films was investigated by GIWAXD measurements, which were performed on the X9 beamline at the National Synchrotron Light Source (NSLS, Upton, NY, USA), Brookhaven National Laboratory. The wavelength (λ) and incident angle (θ_s) of X-ray beams were 0.0918 nm and 0.11°, respectively. Since the critical angle of the total reflection for the *i*PP film is calculated to be 0.08°, the diffraction pattern is supposed to reflect the structure of the entire region of the film in terms of the depth direction. An azimuthal plot was obtained from a two-dimensional GIWAXD pattern.

The aggregation states of *i*PP and *a*PP at the substrate interface were examined by SFG spectroscopy. SFG spectra were collected with the visible and IR beams traveling through the prism and overlapping at the center of the sample. The incident angles for the visible and IR beams were 55° and 65° from the surface normal, respectively. The intensity of SFG signals (I^{SFG}) is proportional to the square of the absolute value of the effective sum-frequency susceptibility tensor of the interface ($\chi_{eff}^{(2)}$),

$$I^{SFG} \propto \left|\chi_{eff}^{(2)}\right|^2 I_{Vis} I_{IR} \quad (1)$$

where I_{vis} and I_{IR} are the intensity of the visible and IR lasers, respectively. Thus, the intensity of the SFG signals was normalized by those of the original visible and IR beams. The measurements were taken at room temperature with the *ssp* (SF output, visible input, and infrared input) polarization combination. A more detailed explanation of the experimental setup is described in the ESI.

Figure 1 shows the AFM topographic and phase images for spin-coated *i*PP thin films with thicknesses of 180, 80 and 35 nm. For the 180 nm- and 80 nm-thick films, lamellar fibrils in a spherulite were observed. However, in the case of the 35 nm-thick film, such a morphology was not observed. This can be explained in terms of the restricted crystal growth due to the strong confinement effect.[60, 61] These results imply that the aggregation states of crystalline lamellae, which are constituents of the fibrils, in the 35 nm-thick film were different from those of the thicker ones.

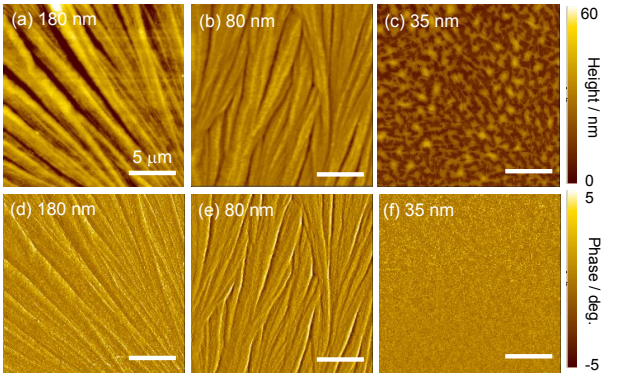

Figure 1. AFM topographic and phase images for (a, d) 180 nm-thick, (b, e) 80 nm-thick, and (c, f) 35 nm-thick *i*PP films.

Figure 2 shows the two-dimensional GIWAXD patterns for spin-coated *i*PP thin films with thicknesses of 180, 80 and 35 nm. In the case of the 180 nm-thick *i*PP film, an arc was observed at the scattering vector q (= $4\pi\sin\theta_s/\lambda$) = 10.0 nm^{-1} both along the in-plane and out-of-plane directions. Similarly, an arc at q = 12.0 nm^{-1} was observed in the in-plane and out-of-plane directions. The diffraction arcs at 10.0 and 12.0 nm^{-1} can be assigned to (110) and (040) of the α form, respectively, as indicated in

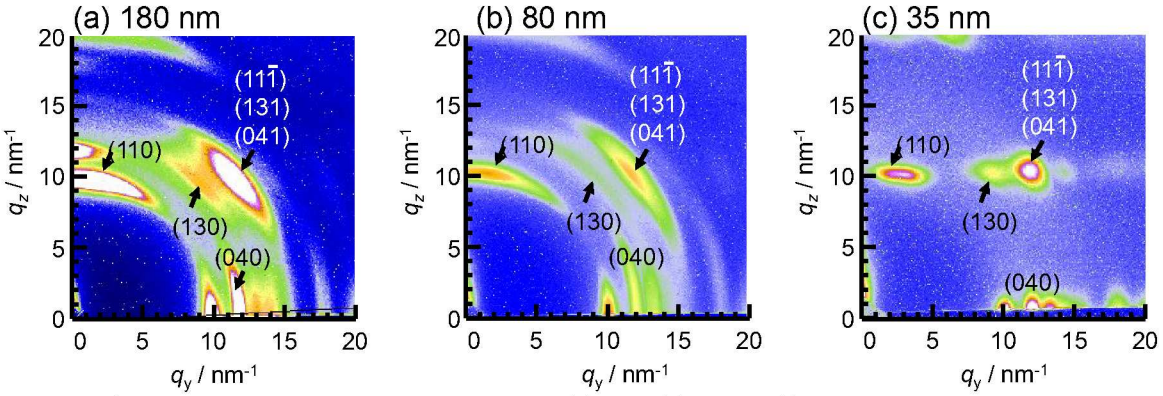

Figure 2. GIWAXD patterns for *i*PP films with thicknesses of (a) 180 nm, (b) 80 nm, and (c) 35 nm with an incident angle of 0.11°.

Figure 1.[62-64] Arcs were also observed at q = 13.1 and 15.1 nm^{-1} in the diagonal direction, which could be assigned to (130) and the mixture of (11$\bar{1}$), (131) and (041) of the α form.[62-64] The GIWAXD pattern for the 80 nm-thick film was similar to the 180 nm-thick one but the magnitude of diffraction intensity was much weaker due to the smaller scattering volume. However, as the film was further thinned to 35 nm, diffraction spots were observed instead of the arcs, indicating the formation of highly ordered lamellar crystals within the film compared to those of the thicker films.

The orientation of crystalline lamellae was then examined. Figure S1 shows the azimuthal angle dependence of relative intensity of (a) (040) and (b) (110) reflections for the *i*PP films of various thicknesses. For all the samples, the (040) and (110) reflections were observed around an equator (q_z ~ 0 nm^{-1}). This (040) reflection indicates that the *b*-axis oriented along the direction parallel to the substrate interface. Besides, since the (040) and (110) are the zone planes of [001] zone axis, these reflections suggested that the *c*-axis oriented along the direction perpendicular to the substrate interface. In other words, the lamellae were oriented face-on. On the other hand, the (110) reflection was also observed at the off-axis apart from the meridian (q_y ~ 2 nm^{-1} and q_z ~ 10 nm^{-1}) for all of the samples. Taking the *b*-axis oriented along the direction parallel to the substrate interface, this indicates that the *c*-axis oriented along the direction parallel to the substrate interface. This means that the edge-on lamellae also existed. Thus, it is most likely that *i*PP formed an orthogonal cross-hatched lamellar structure, where daughter lamellae epitaxially grew on the *ac* plane of mother lamellae, as previously reported.[65-67] Since the (110) reflection from the face-on lamellae (the in-plane reflection) was stronger than that from the edge-on lamellae (the off-axis reflection), as shown in Figure S1, the face-on orientation seems to be dominant, namely, the mother lamellae. Figure 3 shows a schematic drawing of the crystalline lamellae, which satisfies the diffraction patterns for the 35 nm-thick film. It should be noted that the (040) reflection was observed around the meridian for the 180 nm-thick film. This makes it clear that the edge-on lamellae were also contained in the 180 nm-thick film. Thus, it can be claimed that the crystal orientation in the *i*PP thin films changed from a mixture of edge-on and face-on mother lamellae to preferential face-on mother lamellae with decreasing film thickness. This was consistent with previous reports.[60, 61, 67]

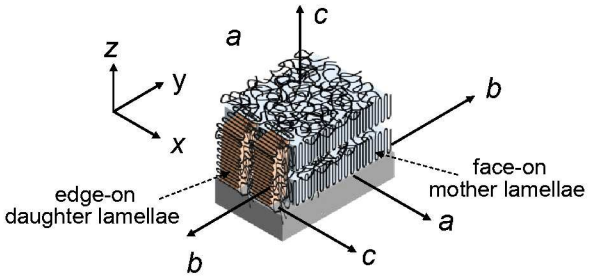

Figure 3. Schematic illustration of a crystalline lamellar orientation for the 35 nm-thick film.

For the thermodynamic factor, the free energy of a primary nucleus for edge-on and face-on lamellae at the surface and substrate interface was calculated (ESI). As a result, the face-on lamellae would be preferentially formed as the crystallization was initiated and proceeded at the silicon interface. Assuming that the face-on mother lamellae were formed at first and then branching of the lamellae occurred, our results can be basically explained in terms of the thermodynamic factor.

The surface orientation of the lamellae has been extensively studied mainly by AFM.[20, 44-46] However, the selective observation of the lamellar orientation in the interior region of the film is difficult to accomplish. SFG provides vibrational information at places where centrosymmetry is broken.[49, 68] This enables the technique to gain direct access to the local conformation of polymer chains at various interfaces.[51, 52, 54, 56, 57, 69-71] If such information at crystal/amorphous interfaces buried in the *i*PP film is accessible by SFG, discussion about the lamellar orientation in the interior region of the film becomes possible.

Figure 4(a) and (b) show SFG spectra for films of *i*PP and *a*PP which is amorphous for comparison, respectively, with various thicknesses. For clarity, each spectrum was vertically shifted. In addition, the signal intensity for the 80 nm- and 35 nm-thick *i*PP films was multiplied by 5 and 20 times, respectively. While the most prominent peak for the *i*PP film was detected at 2,845 cm^{-1}, which was assignable to the symmetric C-H stretching vibration of methylene groups (CH_2s),[72, 73] respectively, the

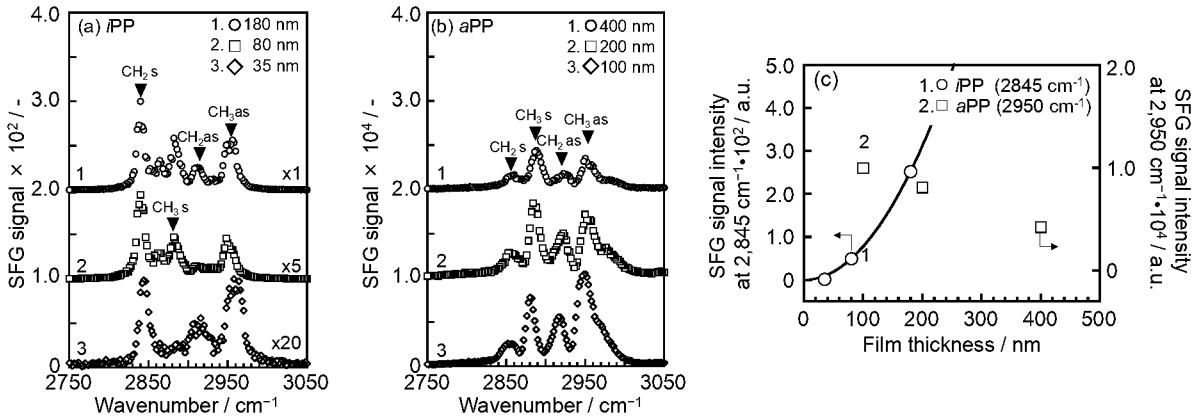

Figure 4. SFG *ssp* spectra for (a) *i*PP and (b) *a*PP films with various thicknesses. In panel (a), the SFG signal for the 80 nm-thick and 35 nm-thick *i*PP films was multiplied by 5 and 20 times, respectively. (c) SFG signal intensity at 2,845 cm^{-1} for *i*PP and at 2,950 cm^{-1} for *a*PP as a function of film thickness. A solid curve is drawn to fit the data for the *i*PP films using a simple quadratic function.

intense peaks for the *a*PP film were the symmetric and anti-symmetric C-H stretching vibrations of methyl groups (CH_3s and CH_3as) at 2,884 and 2,950 cm^{-1}.[73] A peak observed at 2,915 cm^{-1} was assignable to the anti-symmetric C-H stretching of methylene groups (CH_2as).[72] Although the CH_3s peak was observed for both the 180 nm- and 80 nm-thick films, it was not for the 35 nm-thick film.

Figure 4(c) shows the thickness dependence of the signal intensity of CH_2s for *i*PP films and CH_3as for *a*PP ones. The SFG signal intensity for the *a*PP film decreased with increasing film thickness. Under the current measurement conditions and especially for the incident angles of the excited IR and visible beams, the contribution to the SFG signals from the air surface was greater than that from the substrate interface. As IR beams travel from the substrate interface through the film, they are partially absorbed on the way to the air surface. Taking into account that the intensity of SFG signals is proportional to that of IR as shown by eq. (1), the thickness dependence of SFG signals observed for the *a*PP film can be understood. In contrast, in the case of the *i*PP film, SFG signals increased with increasing thickness. This implies that signals are generated from not only the air surface and the substrate interface but also buried crystal/amorphous interfaces in which the amount is proportional to the thickness. The following two paragraphs lend support to this theory.

Ye *et al.* conducted an SFG study for an arachidic acid Langmuir-Blodgett (LB) film and claimed that the SFG signal intensity was proportional to the square of the number (n) of layers.[74] As the non-resonant term for the susceptibility is negligible, the I^{SFG} for the LB film can be given by,

$$I^{\mathrm{SFG}} \propto n^2 \left|\chi_{\mathrm{n}}^{(2)}\right|^2 \qquad (2)$$

where $\chi_n^{(2)}$ is the nonlinear susceptibility in the nth layer. Given that the number of crystal/amorphous interfaces is simply proportional to the film thickness, the I^{SFG} for the *i*PP film is supposed to be proportional to the square of the thickness. This is actually what is shown in Figure 4 (c), in which a solid line drawn by a simple quadratic function well fits the data for the *i*PP film.

Here, for clarity, the weight of the contribution to the SFG signals from the crystal/amorphous interfaces is discussed. The $\chi^{(2)}_{eff}$ values at the quartz/*i*PP, *i*PP/air, *i*PP(amorphous region)/*i*PP (crystal, *a*-axis direction) and *i*PP(amorphous region)/*i*PP(crystal, *c*-axis direction) interfaces were calculated to be 0.46, 1.61, 0.50 and 0.38, respectively (see the ESI). Since the $\chi^{(2)}_{eff}$ values at the crystal/amorphous interface were comparable to those at the quartz/*i*PP interface, the SFG signals generated from the crystal/amorphous interfaces buried in the *i*PP film can be detected, as discussed in the above.

Figure 5 shows the thickness dependence of the intensity ratio of CH_3s to CH_3as (I_{CH3s}/I_{CH3as}). The I_{CH3s}/I_{CH3as} values for the 180 nm- and 80 nm-thick films were comparable to each other and larger than that for the 35 nm-thick film. This result corresponds to the GIWAXD results where only the 35 nm-thick film exhibited a different crystalline orientation. Thus, it can be claimed that the orientation of CH_3 groups changed accompanied by a change in the lamellar orientation.

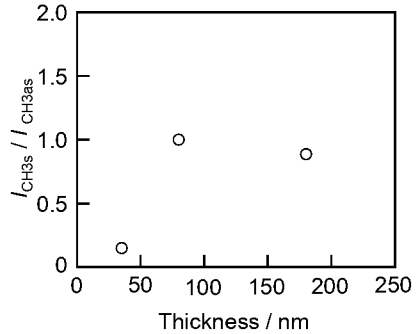

Figure 5. SFG intensity ratio of CH_3s and CH_3as modes as a function of film thickness.

The tilt angle (θ), twist angle (ψ) and azimuthal angle (φ) of a CH_3 group with a direction normal to the interface can be examined in principle using the I_{CH3s}/I_{CH3as} value.[75] Unfortunately however, the simulation with θ as a fitting parameter and constant ψ and φ values could not reproduce the experimental data. Interfacial chains can be roughly classified into two groups; those that are partially incorporated into

crystalline lamellae and those that are not. The former is further divided into ones in the crystalline and amorphous phases, while the latter is in the amorphous phase. The local conformation of chains in the crystalline phase is correlated with the crystal unit cell and its orientation. In the amorphous part of chains which are connected into a lamella, tie- and loop-conformations are contained.[43, 76] Segments of a tie-chain are simply oriented along the direction perpendicular to the interface. However, those in a loop-chain are first oriented perpendicular to the interface and then in parallel. Hence, the obtained SFG signals can be the sum of the contributions from the above-mentioned partial chains. The current available model to simulate the local orientation of CH_3 groups is not simply applicable to such a complex system. To clarify the difficulty, a simpler system such as a single crystal of polymers with a well-defined folding structure is necessary. This kind of experiment will be designed in the future.

Conclusions

In conclusion, the aggregation states of *i*PP in spin-coated thin films were examined by GIWAXD in conjunction with SFG measurements. GIWAXD measurements revealed that the crystal orientation in the *i*PP thin films changed from a mixture of edge-on and face-on lamellae to preferential face-on lamellae with decreasing film thickness. This could be explained in terms of the thermodynamic factor. We then demonstrated that SFG spectroscopy was applicable to characterize *i*PP chains at the crystal/amorphous interfaces in the interior region of the thin films. The orientation of CH_3 groups at the crystal/amorphous interfaces varied for an ultrathin film, accompanied by a change in the lamellar orientation.

Conflicts of interest

There are no conflicts to declare.

Acknowledgements

This work was supported by JSPS KAKENHI for Scientific Research (B) (No. JP20H02790) to KT and Scientific Research (B) (No. JP20H02802) to DK from the Ministry of Education, Culture, Sports, Science, and Technology (MEXT), Japan. We are also thankful for the support from the JST-Mirai Program (JPMJMI18A2). This research used Beamline X9 of the National Synchrotron Light Source, a U.S. Department of Energy (DOE) Office of Science User Facility operated for the DOE Office of Science by Brookhaven National Laboratory Under Contracts No. DE-AC02-98CH10886.

Notes and references

1. O. K. C. Tsui and T. P. Russell, *Polymer Thin Films*, World Scientifc, Singapore, 2008.
2. J. L. Keddie, R. A. L. Jones and R. A. Cory, *Faraday Discuss.*, 1994, **98**, 219-230.
3. W. E. Wallace, J. H. van Zanten and W. L. Wu, *Phys. Rev. E*, 1995, **52**, R3329-R3332.
4. P. Rittigstein, R. D. Priestley, L. J. Broadbelt and J. M. Torkelson, *Nat. Mater.*, 2007, **6**, 278-282.
5. K. Tanaka, Y. Tateishi, Y. Okada, T. Nagamura, M. Doi and H. Morita, *J. Phys. Chem. B*, 2009, **113**, 4571-4577.
6. S. Napolitano and M. Wübbenhorst, *Nat. Commun.*, 2011, **2**, 260.
7. Y. Fujii, H. Morita, A. Takahara and K. Tanaka, in *Glass Transition, Dynamics and Heterogeneity of Polymer Thin Films*, ed. T. Kanaya, 2013, vol. 252, pp. 1-27.
8. K. Chrissopoulou and S. H. Anastasiadis, *Soft Matter*, 2015, **11**, 3746-3766.
9. M. Inutsuka, A. Horinouchi and K. Tanaka, *ACS Macro Lett.*, 2015, **4**, 1174-1178.
10. K. Matsuura, Y. Matsuda and S. Tasaka, *Polym. J.*, 2018, **50**, 375-380.
11. H. Jinnai, *Polym. J.*, 2018, **50**, 1121-1138.
12. H. K. Nguyen, S. Sugimoto, A. Konomi, M. Inutsuka, D. Kawaguchi and K. Tanaka, *ACS Macro Lett.*, 2019, **8**, 1006-1011.
13. G. Reiter and J.-U. Sommer, *Phys. Rev. Lett.*, 1998, **80**, 3771-3774.
14. D. A. Ivanov, Z. Amalou and S. N. Magonov, *Macromolecules*, 2001, **34**, 8944-8952.
15. K. Taguchi, H. Miyaji, K. Izumi, A. Hoshino, Y. Miyamoto and R. Kokawa, *Polymer*, 2001, **42**, 7443-7447.
16. M. Wang, H.-G. Braun and E. Meyer, *Macromol. Rapid Commun.*, 2002, **23**, 853-858.
17. H. G. Haubruge, R. Daussin, A. M. Jonas and R. Legras, *Polymer*, 2003, **44**, 8053-8059.
18. H. Schönherr and C. W. Frank, *Macromolecules*, 2003, **36**, 1199-1208.
19. Y. Liang, M. Zheng, K. H. Park and H. S. Lee, *Polymer*, 2008, **49**, 1961-1967.
20. V. H. Mareau and R. E. Prud'homme, *Macromolecules*, 2005, **38**, 398-408.
21. C. Qiao, J. Zhao, S. Jiang, X. Ji, L. An and B. Jiang, *J. Polym. Sci., Part B: Polym. Phys.*, 2005, **43**, 1303-1309.
22. X. Zhai, W. Wang, G. Zhang and B. He, *Macromolecules*, 2006, **39**, 324-329.
23. Y. Ma, W. Hu and G. Reiter, *Macromolecules*, 2006, **39**, 5159-5164.
24. X. Wang, W. Hou, J. Zhou, L. Li, Y. Li and C.-M. Chan, *Colloid. Polym. Sci.*, 2007, **285**, 449-455.
25. T. J. Zimudzi and M. A. Hickner, *ACS Macro Lett.*, 2016, **5**, 83-87.
26. D. I. Kushner, A. Kusoglu, N. J. Podraza and M. A. Hickner, *Adv. Funct. Mater.*, 2019, **29**, 1902699.
27. M. Tariq, O. Dolynchuk and T. Thurn-Albrecht, *J. Phys. Chem. C*, 2020, **124**, 26184-26192.
28. C. W. Frank, V. Rao, M. M. Despotopoulou, R. F. W. Pease, W. D. Hinsberg, R. D. Miller and J. F. Rabolt, *Science*, 1996, **273**, 912-915.
29. Y. Wang, C.-M. Chan, K.-M. Ng and L. Li, *Macromolecules*, 2008, **41**, 2548-2553.
30. K. Jeon and R. Krishnamoorti, *Macromolecules*, 2008, **41**, 7131-7140.
31. H. Sirringhaus, P. J. Brown, R. H. Friend, M. M. Nielsen, K. Bechgaard, B. M. W. Langeveld-Voss, A. J. H. Spiering, R. A. J. Janssen, E. W. Meijer, P. Herwig and D. M. de Leeuw, *Nature*, 1999, **401**, 685-688.

32. J.-F. Chang, B. Sun, D. W. Breiby, M. M. Nielsen, T. I. Sölling, M. Giles, I. McCulloch and H. Sirringhaus, *Chem. Mater.*, 2004, **16**, 4772-4776.
33. D. M. DeLongchamp, B. M. Vogel, Y. Jung, M. C. Gurau, C. A. Richter, O. A. Kirillov, J. Obrzut, D. A. Fischer, S. Sambasivan, L. J. Richter and E. K. Lin, *Chem. Mater.*, 2005, **17**, 5610-5612.
34. R. Joseph Kline, M. D. McGehee and M. F. Toney, *Nat. Mater.*, 2006, **5**, 222-228.
35. M. Brinkmann, *J. Polym. Sci. Polym. Phys.*, 2011, **49**, 1218-1233.
36. B. Huang, E. Glynos, B. Frieberg, H. Yang and P. F. Green, *ACS Appl. Mater. Interfaces*, 2012, **4**, 5204-5210.
37. V. Skrypnychuk, N. Boulanger, V. Yu, M. Hilke, S. C. B. Mannsfeld, M. F. Toney and D. R. Barbero, *Adv. Funct. Mater.*, 2015, **25**, 664-670.
38. D. Kajiya, S. Ozawa, T. Koganezawa and K.-i. Saitow, *J. Phys. Chem. C*, 2015, **119**, 7987-7995.
39. Y. Ogata, D. Kawaguchi and K. Tanaka, *Sci. Rep.*, 2015, **5**.
40. Y. Ogata, D. Kawaguchi and K. Tanaka, *J. Phys. Chem. Lett.*, 2015, **6**, 4794-4798.
41. T. Abe, D. Kawaguchi, M. Watanabe, T. Hoshino, T. Ishihara and K. Tanaka, *Appl. Phys. Lett.*, 2021, **118**, 181601.
42. M. Takayanagi, K. Imada and T. Kajiyama, *J. Polym. Sci. Part C Polym. Symp.*, 1967, **15**, 263-281.
43. H. D. Keith, F. J. Padden Jr. and R. G. Vadimsky, *J. Polym. Sci. Polym. Phys.*, 1966, **4**, 267-281.
44. L. Li, C.-M. Chan, K. L. Yeung, J.-X. Li, K.-M. Ng and Y. Lei, *Macromolecules*, 2001, **34**, 316-325.
45. Y. Kikkawa, H. Abe, M. Fujita, T. Iwata, Y. Inoue and Y. Doi, *Macromol. Chem. Phys.*, 2003, **204**, 1822-1831.
46. Y. Jiang, D.-D. Yan, X. Gao, C. C. Han, X.-G. Jin, L. Li, Y. Wang and C.-M. Chan, *Macromolecules*, 2003, **36**, 3652-3655.
47. P. C. Jukes, A. Das, M. Durell, D. Trolley, A. M. Higgins, M. Geoghegan, J. E. Macdonald, R. A. L. Jones, S. Brown and P. Thompson, *Macromolecules*, 2005, **38**, 2315-2320.
48. M. Asada, N. Jiang, L. Sendogdular, P. Gin, Y. Wang, M. K. Endoh, T. Koga, M. Fukuto, D. Schultz, M. Lee, X. Li, J. Wang, M. Kikuchi and A. Takahara, *Macromolecules*, 2012, **45**, 7098-7106.
49. Y. R. Shen, *Nature*, 1989, **337**, 519-525.
50. Z. Chen, Y. R. Shen and G. A. Somorjai, *Annu. Rev. Phys. Chem.*, 2002, **53**, 437-465.
51. Y. Tateishi, N. Kai, H. Noguchi, K. Uosaki, T. Nagamura and K. Tanaka, *Polym. Chem.*, 2010, **1**, 303-311.
52. H. Tsuruta, Y. Fujii, N. Kai, H. Kataoka, T. Ishizone, M. Doi, H. Morita and K. Tanaka, *Macromolecules*, 2012, **45**, 4643-4649.
53. S. Shimomura, M. Inutsuka, K. Tajima, M. Nabika, S. Moritomi, H. Matsuno and K. Tanaka, *Polym. J.*, 2016, **48**, 949-953.
54. H. K. Nguyen, M. Inutsuka, D. Kawaguchi and K. Tanaka, *ACS Macro Lett.*, 2018, **7**, 1198-1202.
55. M. Sen, N. S. Jiang, M. K. Endoh, T. Koga, A. Ribbe, A. Rahman, D. Kawaguchi, K. Tanaka and D. M. Smilgies, *Macromolecules*, 2018, **51**, 520-528.
56. S. Sugimoto, M. Inutsuka, D. Kawaguchi and K. Tanaka, *ACS Macro Lett.*, 2018, **7**, 85-89.
57. B. Zuo, M. Inutsuka, D. Kawaguch, X. P. Wang and K. Tanaka, *Macromolecules*, 2018, **51**, 2180-2186.
58. K. Yamamoto, D. Kawaguchi, K. Sasahara, M. Inutsuka, S. Yamamoto, K. Uchida, K. Mita, H. Ogawa, M. Takenaka and K. Tanaka, *Polym. J.*, 2019, **51**, 247-255.
59. S. Mori and H. G. Barth, *Size Exclusion Chromatography*, Springer, Berlin, 1999.
60. B. Zhang, J. Chen, B. Liu, B. Wang, C. Shen, R. Reiter, J. Chen and G. Reiter, *Macromolecules*, 2017, **50**, 6210-6217.
61. C. Luo, M. Kröger and J.-U. Sommer, *Polymer*, 2017, **109**, 71-84.
62. E. J. Addink and J. Beintema, *Polymer*, 1961, **2**, 185-193.
63. A. T. Jones, J. M. Aizlewood and D. R. Beckett, *Makromol. Chem.*, 1964, **75**, 134-158.
64. Z. Mencik, *Journal of Macromolecular Science, Part B*, 1972, **6**, 101-115.
65. F. J. Padden Jr. and H. D. Keith, *J. Appl. Phys.*, 1973, **44**, 1217-1223.
66. K. Yamada, S. Matsumoto, K. Tagashira and M. Hikosaka, *Polymer*, 1998, **39**, 5327-5333.
67. K. Uchida, K. Mita, Y. Higaki, K. Kojio and A. Takahara, *Polym. J.*, 2019, **51**, 183-188.
68. J. H. Hunt, P. Guyot-Sionnest and Y. R. Shen, *Chem. Phys. Lett.*, 1987, **133**, 189-192.
69. A. Horinouchi, H. Atarashi, Y. Fujii and K. Tanaka, *Macromolecules*, 2012, **45**, 4638-4642.
70. M. Sen, N. Jiang, J. Cheung, M. K. Endoh, T. Koge, D. Kawaguchi and K. Tanaka, *ACS Macro Lett.*, 2016, **5**, 504-508.
71. H. K. Nguyen, M. Inutsuka, D. Kawaguchi and K. Tanaka, *J. Chem. Phys.*, 2017, **146**, 203313.
72. D. Zhang, Y. R. Shen and G. A. Somorjai, *Chem. Phys. Lett.*, 1997, **281**, 394-400.
73. M. Arruebarrena de Báez, P. J. Hendra and M. Judkins, *Spectrochim. Acta. A*, 1995, **51**, 2117-2124.
74. T. Nishida, C. M. Johnson, J. Holman, M. Osawa, P. B. Davies and S. Ye, *Phys. Rev. Lett.*, 2006, **96**, 077402.
75. C. Hirose, N. Akamatsu and K. Domen, *J. Chem. Phys.*, 1992, **96**, 997-1004.
76. J. D. Hoffman and R. L. Miller, *Polymer*, 1997, **38**, 3151-3212.